



Effect of Laser Energies on the Performance of Exfoliation and Fragmentation for Hexagonal Boron Nitride by Laser

¹Mayyadah H. Mohsin*, ¹Khawla S. Khashan, ¹Ghassan M. Sulaiman, ^{2,3}Khalil A. A. Khalil

¹Department of Applied Sciences, University of Technology – Iraq

²Department of Medical Laboratory Sciences, College of Applied Medical Sciences, University of Bisha – Saudi Arabia

³Department of Medical Laboratory Sciences, Faculty of Medicine and Health Sciences, University of Hodeidah – Yemen

Article information

Article history:

Received: May, 16, 2023

Accepted: August, 05, 2023

Available online: September, 10, 2023

Keywords:

Laser exfoliation,
Laser fragmentation,
H-Boron nitride,
Nano flake,
Nano sheet

*Corresponding Author:

Mayyadah H. Mohsin

mayyadah.h.mohsin@uotechnology.edu.iq

Abstract

A technique for exfoliating Boron nitride (BN) nanosheets was devised, which was then followed by a laser ablation-fragmentation process to produce lamellar hexagonal Boron nitride nanostructures (h-BNNs). The physicochemical properties of the nanoparticles were analyzed to investigate the effect of laser energy and wavelength in the two-step pre-treatment procedure during BN synthesis. The X-ray diffraction (XRD) patterns showed no impurity phase structures and only primary h-BN reflections were visible. It was discovered that the crystallite h-BNNs size ranged from 11 to 18 nm, and nanosecond laser energy was sufficient to transform BN into h-BNNs and a few nanotubes. Combining laser intensity and wavelength transformed the BN nanoparticle shape from haphazardly arranged platelets to melting-like formations. Fourier Transform infrared (FTIR) spectroscopy confirmed distinct observed changes in the size and melting behavior in the h-BNNs and the sharp absorption peaks which could indicate changes in their optical properties. Morphological characteristics and formation of the hexagonal phase of BN caused variations in optical properties and high-resolution transmission electron microscopy (HRTEM) results. Photoluminescence of h-BNNs was observed in the 250–600 nm range with peak emission at 485 nm. Due to its significant structural disorder, the h-BNNs exhibited a wide emission with a strong luminescence that remained largely continuous after 48 hours, resulting in a distinctive blue hue (470, and 485nm).

1. Introduction

Quantum dots also called (QD), containing the compound graphene quantum dots (GQD) and nanodots of carbon have distinctive both chemical and physical characteristics. That makes them ideal for a variety of apps

like photocatalysis, sensor technology, bioimaging, bio-labelling, conversion of energy, and delivery of drugs. As the demand for these QD continues to grow, researchers are exploring Black phosphorus quantum dots (BPQD) and boron nitride quantum dots (BNQD) are two new forms of quantum dots, which offer exceptional features resulting from their size, shape, edge, and layer [1]. A significant increase in interest has been seen in BNQD in particular because of their distinct structure and intriguing physical and chemical characteristics. Created BNQD self-assembled from boron nitride (BN) nanosheets that had undergone exfoliation by high-intensity ultra-sonic [1]. Nanostructures made of hexagonal boron nitride (h-BN) have a specific crystal structure that has piqued the interest of scientists, as it closely resembles that of graphite/graphene (sp^2) h-BN, often known as "white graphene," is isoelectronic with graphene and comprises an equal amount of atoms of nitrogen (N) and boron (B), which form strong sp^2 covalent bonds within each layer. The forces generated by Van der Waals between the layers are weak. Due to its wide band gap range from 4-6 eV, hexagonal Boron nitride nanostructures (h-BNNs) are insulating materials, with electrical insulation demonstrated between the lowest unoccupied molecular orbit (LUMO) in a hexagonal arrangement and the highest occupied molecular orbit (HOMO). Additionally, neighboring h-BN layers may connect via lip-lip ionic bonding interactions [2, 3]. The characteristics of h-BN can be enhanced when the dimension is reduced to the nanoscale, much like graphene nanosheets. Exfoliating BNNs from bulk BN is therefore far more difficult than doing the same for graphene from bulk graphite. BN has been considered the perfect material for creating and manufacturing various nanodevices for the past few decades. The combination of BNQD with h-BNNs inherent qualities, including excellent thermal conductivity, superior stability in chemicals, great luminescence properties, low toxicity, and good dispersibility, has made them promising candidates for use in optical electronic devices [4-6], Far-ultraviolet light-emitting devices, lubrication [5], bio-medicine [6], and Sensors application [7]. The usage of the few-layer Tow dimension (2D) equivalents, however, are more complex. Because pure h-BN retains a significant amount of its crystallinity, top-down techniques including mechanical cleavage, chemical modification, and liquid phase separation by sonication have been favored to exfoliate BN multilayer materials [8, 9]. A practical method for creating well-controlled h-BN nanosheets or nanoparticles with a surface activity that supports certain characteristics is pulse laser ablation in liquid (PLAL), particularly for optic applications. Meanwhile, laser exfoliation in solution (LES) provides an easy, quick, and environmentally friendly method for creating various nanomaterials by concentrating a laser beam on a powder dispersion in an aqueous solution, LES produces nanomaterials compared to bulk targets, with a more homogeneous structure on the surface and a lower size distribution [10]. The preparation of h-BN through laser exfoliation poses certain challenges that need to be addressed for efficient and reliable synthesis compared with other methods such as chemical vapor deposition (CVD), ball milling, and plasma-enhanced chemical vapor deposition (PECVD), among others. One of the primary issues is achieving a high yield of h-BN flakes. The process relies on precise laser energy to cleave the layered material, but it is often difficult to maintain consistent energy levels, leading to varying flake sizes and qualities. Additionally, the scalability of the laser exfoliation process remains a challenge. While small-scale experiments have shown promise, scaling up production to meet industrial demands is complex. Optimizing laser parameters, substrate choice, and deposition techniques are key aspects that need to be thoroughly investigated to enable large-scale, cost-effective synthesis of h-BN. Addressing these problems in preparation for h-BN by laser exfoliation will contribute to advancing the understanding and application of this remarkable material in various fields, including electronics, optics, drug delivery, and energy storage. In this study, we report and focus on the characterization and properties of h-BNNs prepared by a new technique called exfoliation and fragmentation by laser method. The physical-chemical properties of the h-BNNs were thoroughly investigated through surface characterization, determination of morphology, analysis of structures and chemical bonds, and examination of fluorescence and optical properties. These investigations were crucial in revealing the essential characteristics of the h-BNNs we believe that our method offers an easy way to create nanomaterials based on Boron nitride, which has promising applications in the fields of cancer treatment and optoelectronics.

2. Experimental Procedure

The process of synthesizing h-BNNs involved laser exfoliation/fragmentation of BN particles in deionized distilled water (DDW). The resulting h-BNNs were characterized within two hours of production using the same approach as described in a previous study and shown in Figure 1 [4, 11, 12]. To produce BN nanosheets, 20 mg of the h-BN powder with 3–4 μm size particles and 99.99 % purity acquired from Sky Spring Nanomaterials, Inc. The substance was diluted in 50 ml of DDW and subjected to prop sonication for a duration of 10 minutes. The suspension was then laser irradiated at different energies (10, 30, and 50 mJ/pulse) with an Nd: YAG laser

system (central wavelength: 1064 nm, pulse duration: 2 ns, repetition rate: 1 Hz) followed by further laser fragmentation in liquid (532 nm, 50 pulses by the same laser system) to form colloids [11]. After irradiation, to separate the boron nitride nanoparticles from the supernatant and eliminate larger particles, the solution underwent centrifugation at a speed of 4,000 rpm for a duration of five minutes. Colloidal samples were applied to a glass surface and allowed to air dry. The Shimadzu, Inc. X-ray diffractometer (XRD) was used, with Cu-K α radiation at 1.5405 Å, 40 kV, and 25 mA, measuring the diffraction pattern between 20 and 80 over a 2 θ range. The UV absorption spectra of colloidal suspensions within the range of 200–500 nm were measured using a Shimadzu Ultraviolet-2600 spectrophotometer. Using a Nicolet Avatar 360 spectrophotometer, Fourier Transform infrared (FTIR) spectra were collected, while fluorescence emission was measured using a Shimadzu Spectra fluorophotometer model RF-5301pc. The INSPECT F50 Field Emission Scanning Electron Microscopy (FESEM) was used to characterize the dimensions and structural characteristics of h-BNNs. The shape, and size distribution of nanoparticles were investigated using high-resolution transmission electron microscopy (HRTEM) (JEOL-2100F 200 kV), and Selected Area Electron Diffraction (SAED) was used to determine the atomic structure of a crystalline sample.

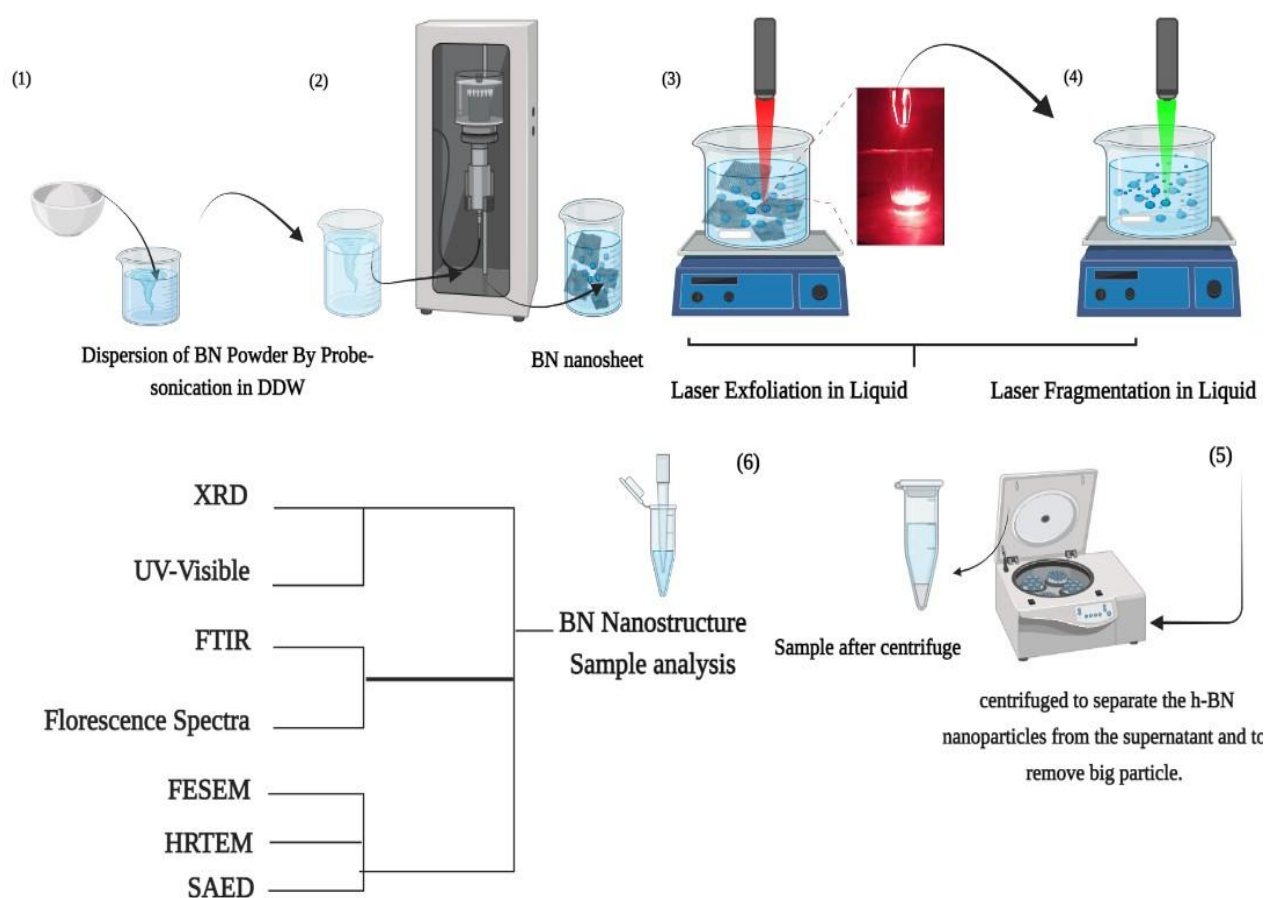


Figure 1: Depicts a schematic view of the preparation h-BNNs method.

3. Results and Discussion

3.1. X-ray Diffraction

Figure 2 shows XRD images of the colloidal solution obtained from a pulsed Nd: YAG laser, using the first (1064 nm) and second harmonics (532 nm). The XRD patterns of the six products were compared to standard patterns of h-BN (JCPDF card number 45-0893 and JCPDS 34-0421), as well as previous studies [13, 14]. The absence of additional peaks indicating impurity phases in the observed pattern confirms the high purity of the synthesized material. Distinctive peaks of h-BN are observed at various diffraction angles, namely (002), (100),

(101), (004), (102), (103), and (110), with the main peak at 26.7° (002) and a weak peak (210) of BN nanotube [12, 15], as shown in Tables 1 and 2.

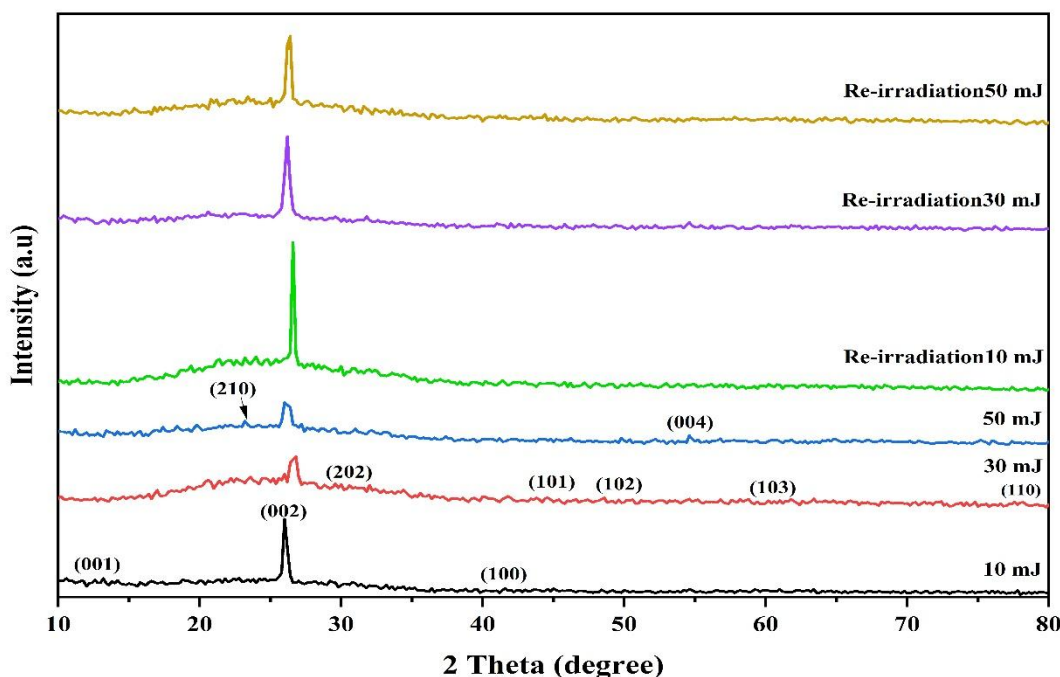


Figure 2: X-ray patterns of h-BNNs synthesized by laser exfoliation by (1066 nm), and fragmentation by (532 nm) in DDW with different laser energy.

In Figure 2, it is clear that the intensities of XRD peaks for the sample prepared using a 1064 nm laser with different energy levels (10, 30, and 50 mJ) decrease. The full width at half maximum (FWHM) of the (002) diffractions also increases, indicating a decrease in the crystalline perfection of the h-BNNs samples with an increase in the pressure due to increasing laser energy. Peak shifts in XRD can be caused by various factors such as changes in lattice parameters, microstrain, crystal size, and nanoparticle size. Nanoparticle size has a significant impact on the diffraction pattern, making it difficult to analyze nanoparticles with crystalline domains below 5 nm due to broad peaks and low signal-to-noise ratios. Furthermore, the XRD analysis indicates that there is an increase in h-BNNs content with higher laser energy, particularly after laser re-irradiation (laser fragmentation using 532 nm) at 10, 30, and 50 mJ laser energy (as shown in Fig. 2). Laser re-irradiation results in a significant increase in oxygen-functional-groups content within the h-BN layer structure, which has been confirmed by FTIR analysis. This observation is consistent with the similarity between the structures of h-BN and graphene. Additionally, the shift in peaks resulting from laser-water interaction causes defects on the surface of h-BNNs. Laser ablation of Boron nitride also generates other BN nanostructures such as BN nanosphere, nanosheets, nanotubes, and nanoflake that detach from BN nanosheets under high temperature and pressure conditions caused by the laser plasma plume. This finding is consistent with the FESEM results discussed in the following section. It can be observed that the three samples exhibit variations in the broadening of diffraction peaks during X-ray analysis, indicating differences in the fine structure of the synthesized nanoparticles. To determine the average grain size (D) of the samples, the Scherrer equation [16, 17] can be utilized:

$$D = 0.9 \lambda / \beta \cos \theta \quad (1)$$

Where λ represents the X-ray wavelength, β represents the full width at half maximum (FWHM) of the diffraction peak, and θ denotes the Bragg angle. The mean grain sizes are given in Tables 1 and 2, D of h-BN (preparation at 1064nm) by Scherrer approximation leads to approximately (18 nm) by 10 mJ, (13 nm) by 30 mJ,

and (18 nm) by 50 mJ in Figure 2A but in Figure 2B, for h-BNNs synthesis after re-irradiation by 532 nm D equal to (11nm) of 10 mJ, (14 nm) of 30mJ, and (16.5 nm) of 50 mJ [18].

Table 1: Peaks analysis data for h-BNNs sample synthesis by laser exfoliation in DDW.

Parameter	Sample	2 θ	FWHM	Crystallite Size (nm)	Average (nm)	hkl
1064nm, 338pulse	10 mJ	14.2	0.473	17	18	001
		26.7	0.352	24		002
		41.6	0.656	13		100
	30 mJ	20.532	0.577	14	13	210
		26.7	0.498	16		002
		41.761	0.6	14		100
		58.274	0.9	10		103
		77.63	0.819	12		110
		77.63	0.819	12		110
	50 mJ	15.711	0.359	23	18	001
		23.207	0.431	20		210
		26.143	0.582	14		002
		49.892	0.472	19		100
		54.641	0.56	16		004
		56.677	0.51	18		103
		77.477	0.578	17		110

Table 2: Peaks analysis data for h-BNNs sample synthesis by laser fragmentation in DDW.

Parameter	Sample	2 θ	FWHM	Crystallite Size (nm)	Average (nm)	hkl
532nm, 50 pulse	10 mJ	19.2	0.856	9	11	001
		23.2	1.47	5		210
		26.585	0.357	23		002
	30 mJ	32.049	0.956	8	14	001
		20.617	0.889	9		210
		26.188	0.394	21		002
		31.766	0.704	11		001
		54.625	0.567	16		004
		54.625	0.567	16		004
	50 mJ	20.989	0.355	23	16.5	001
		23.503	0.645	12		210
		26.314	0.394	21		002
		44.347	0.491	17		100
		50.647	0.948	9		102
		77.818	0.592	17		110

3.2. Field Emission Scanning Electron Microscopy

The surface morphology of h-Boron nitride ultra-fine nanoparticles and nanosheets generated through two-step laser exfoliation and fragmentation in deionized distilled water was analyzed using FESEM in Figures 3 and 4. The morphology of the nanoparticles was found to be influenced by both the energy and wavelength of the laser

pulse, with the h-BNNs appearing spherical and forming disk and sheet-like particles that were attached. Compared to BN powder, laser exfoliation in DDW greatly reduced the thickness of h-BNNS, FE-SEM micrographs revealed that sheet-like structures were generated and attached, with alterations in thickness observed in samples produced at various laser energy levels. As the energy of the laser was increased, the surface morphology became coarser. Despite these variations, all samples exhibited tiny sheet structures that enhanced their exfoliated-like structures. Similar structures have also been traced to BN by other literature reports [18, 19].

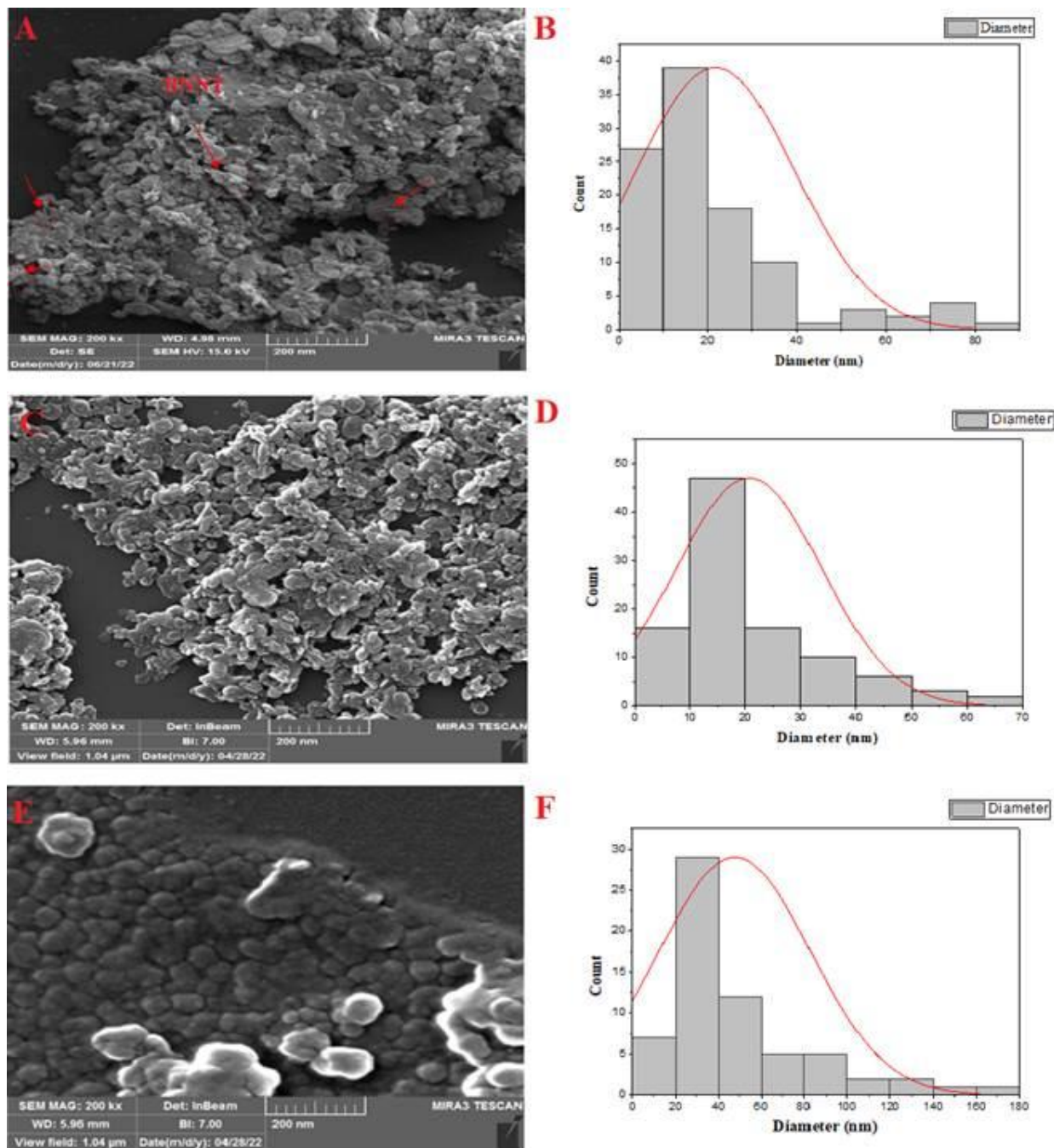


Figure 3: FESEM images of h-BNNs prepared by 1064 nm laser exfoliation in DDW at different laser energy (A (10 mJ), C (30 mJ), and E (50 mJ)), with histogram.

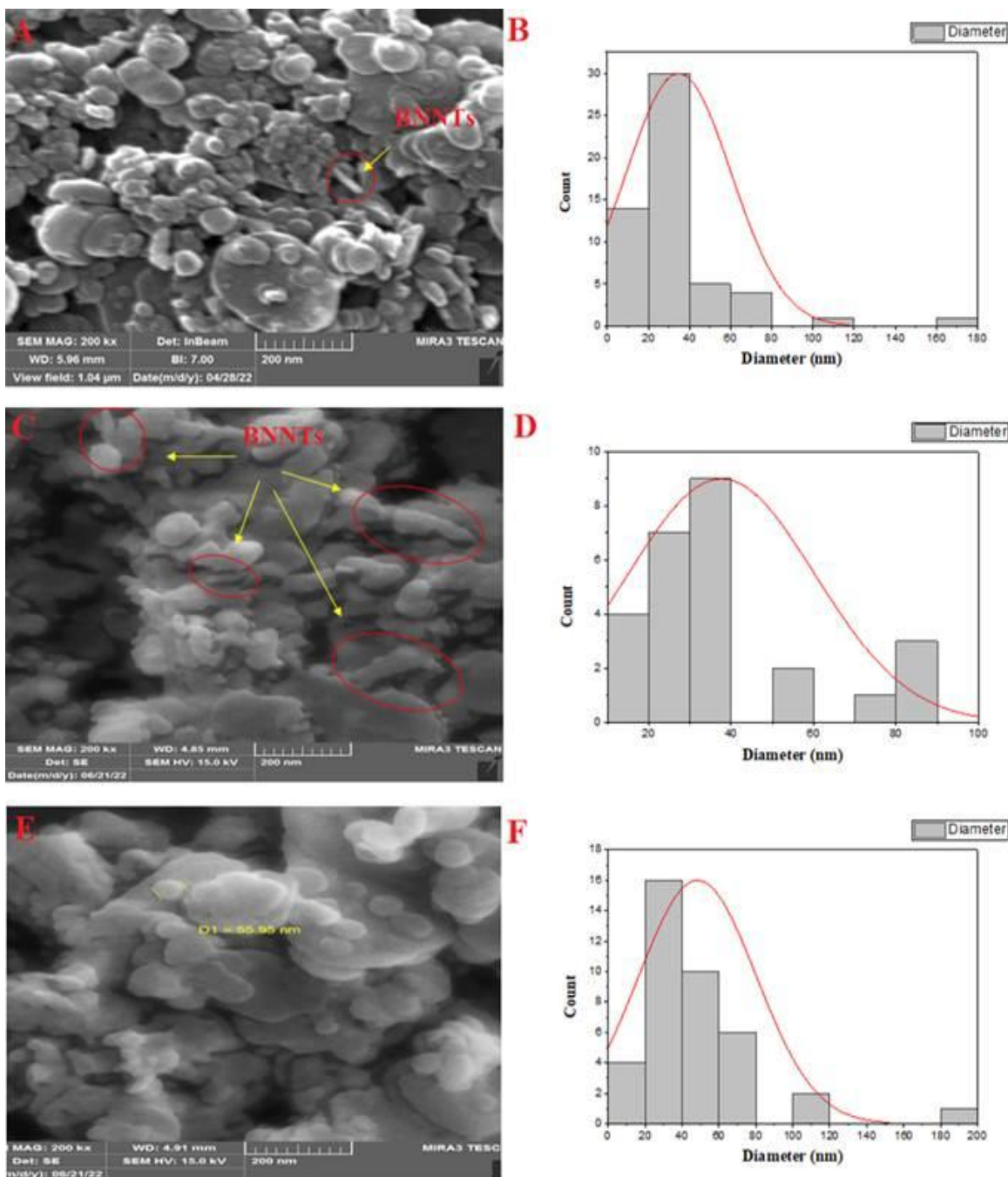


Figure 4: FESEM images of h-BNNs prepared by 532 nm laser fragmentation in deionized DDW at different laser energy (A (10 mJ), C (30 mJ), and E (50 mJ)), with histogram.

The FESEM image reveals that h- BN colloidal nanoparticles aggregate due to multiple factors. Firstly, inter-particle forces play a significant role, including the induced dipole-dipole force between charged particles at polar/non-polar liquid interfaces. This force can be either attractive or repulsive depending on the charges and surface roughness of the particles. Secondly, weak forces cause adhesion between nanoparticles, resulting in (sub) micron-sized entities. The process of agglomeration is governed by thermodynamics and can be influenced by laser energy. The sign of the enthalpy of interaction determines whether poorly agglomerated (repelling) or highly agglomerated (attracting) particle ensembles are formed.

3.3. High-Resolution Transmission Electron Microscopy

The creation of h-BNNS in deionized distilled water involved using various wavelengths and laser energy, with its shape being analysed through HRTEM, and electron diffraction shown in Figures 5, 6, and 7, respectively.

The image of h-BNNS displayed a stacked morphology with a lateral size of a one-micrometer scale and demonstrate that the BNNSs obtained are transparent and evenly distributed, it has been observed that the particles tend to strongly clump together, resulting in significant agglomeration. As a result of this high level of agglomeration, it was not possible to determine the average particle size via the TEM micrograph. Figures 7A and B display the TEM image at low and high magnifications, respectively. The TEM image shows a wrinkled structure with edges resembling graphene and minimal agglomeration. The HRTEM image in Figure 7C shows that the structure of crystals was visible in h-BN, with a 0.21 nm d-spacing and obvious flaws. The distance separating two neighboring B or N atoms in the basal plane of BNNS was found to be 0.21 nm, which is similar to the reported d-spacing of 0.22 nm. We hypothesize that defects in BNNS unclear lattice structure may have resulted from hydrolysis caused by sonication during liquid-phase exfoliation using Nd-YAG lasers (1064 and 532 nm). These exfoliated h-BNNSs can be easily dispersed in an aqueous solution to form a uniform creamy white dispersion that is both stable and homogeneous. The HRTEM micrographs reveal that a wavelength of 532 nm is effective in fragmenting h-BNNs into ultra-nanoparticles of 3-20 nm. These nanoparticles are well-crystallized, as observed from the SAED pattern of h-BNNS displayed in Figures 7D and E. The pattern shows the presence of two sets of hexagonal electron diffraction patterns, indicating that two BN layers are covering each other at an angle of 18° .

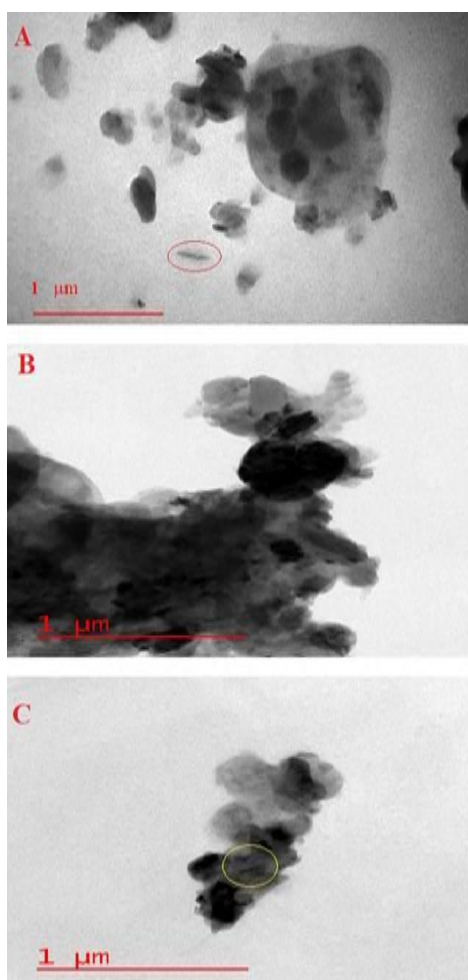


Figure 5: HRTEM images of h-BNNS prepared by 1064 nm pulsed laser exfoliation in DDW at different laser energy (A (10 mJ), B (30 mJ), and C (50 mJ)).

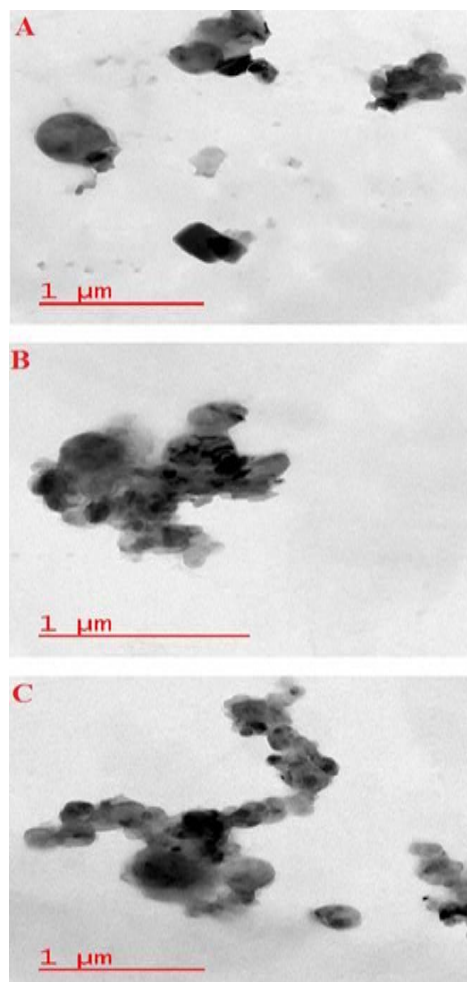


Figure 6: HRTEM images of h-BNNs prepared by 532 nm pulsed laser fragmentation in DDW at different laser energy (A (10 mJ), B (30 mJ), and C (50 mJ)).

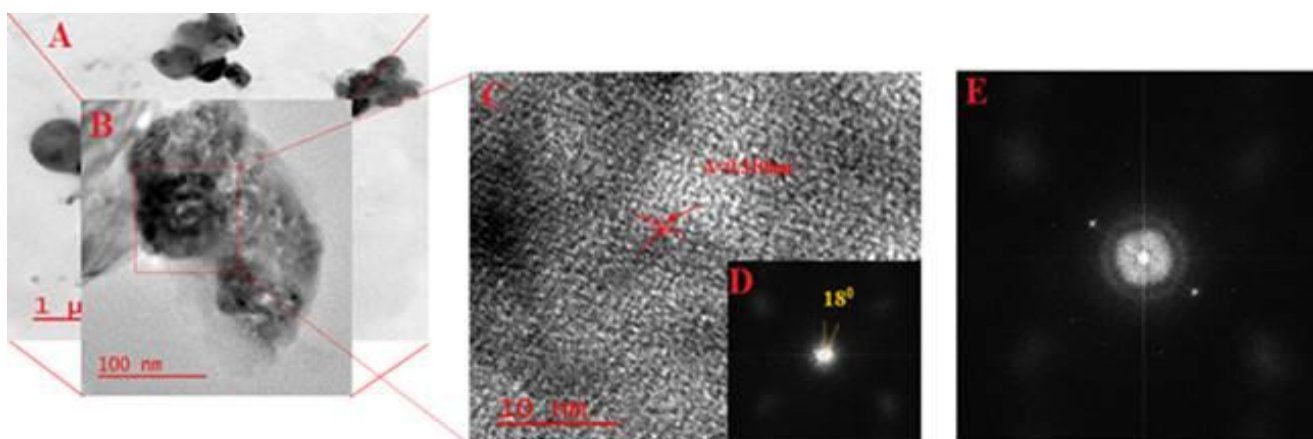


Figure 7: (A, B, and C) HRTEM images of h-BNNs of the sample prepared by laser fragmentation in DDW with 532 nm and 10 mJ (D and E) SAED pattern for h-BNNs.

3.4. Fourier Transform Infrared

FT-IR spectroscopy was used to investigate the changes in the chemical compositions of the reactants. Figures 8 and 9 demonstrate the use of FTIR spectroscopy to elucidate the bonding nature of h-BN ultra-fine nanostructures. The two strong absorption peaks at 600-800 and 1500-1700 cm^{-1} , corresponding to in- the plane B-N-B vibration of bending and in- the plane B-N vibration of stretching, are consistent with the nanoparticles

produced by laser exfoliation and fragmentation in DDW. Additional absorption peaks at 800-1000 and 1300-1400 cm^{-1} are attributed to B-N-B bending, and B-N bending. Peaks at 2125 and 2362 cm^{-1} are ascribed to -CH and C-O bending, respectively. The functional peaks are clearly defined and unambiguous. Water absorption on the sample causes an in-plane band at 3000-3700 cm^{-1} , which corresponds to B-O-H in-plane bending. The presence of oxygen is confirmed by the strong peak at 450-550 cm^{-1} corresponding to O-B-O bending vibration. Vibrations between 1100 and 1300 cm^{-1} in boron oxynitride indicate a transition from BO^2 to BO^- species [19, 20, and 24]. The disappearance of B-N-O and shift of the B-O-B band after increased laser energy indicate that the B-O group Ascbinds to the surface of h-BNNs. A substantial shift in peak positions of h-BN is a direct indication of the covalent bonding of deionized water molecules on the surface of h-BNNs. As stabilized h-BNNs has a band around 500-700 cm^{-1} which indicates O-B-O and B-N bond formation. This confirms the existence of surface oxygen vacancies on boron nitride. The electronic band structures of prepared nanoparticles are strongly influenced by these oxygen vacancies, which will be discussed in Sect. 3.5.

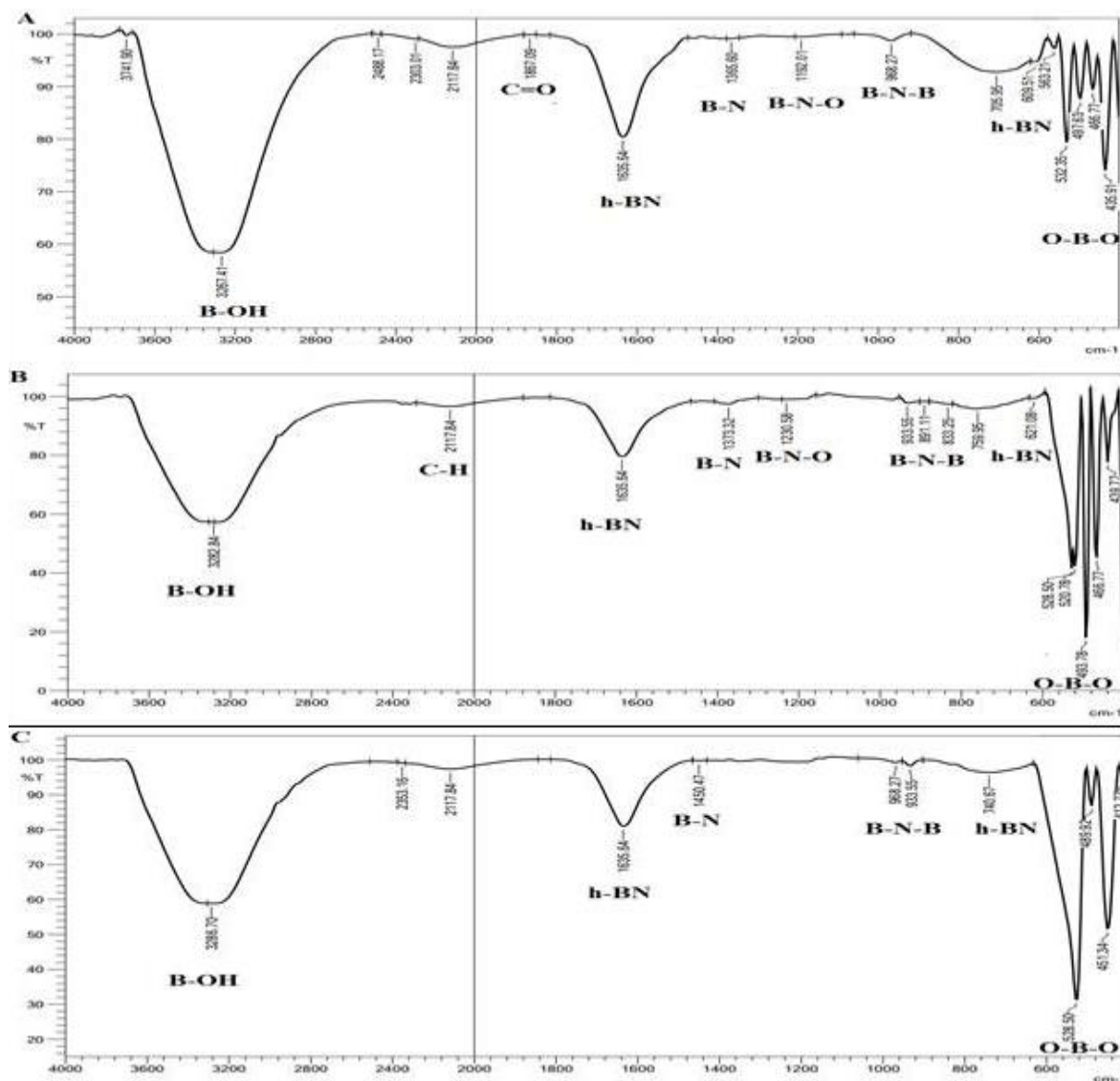


Figure 8: FTIR spectra of h-BNNs colloidal prepared by laser exfoliation by 1064 nm and different laser energy A) 10 mJ, B) 30 mJ, and C) 50 mJ.

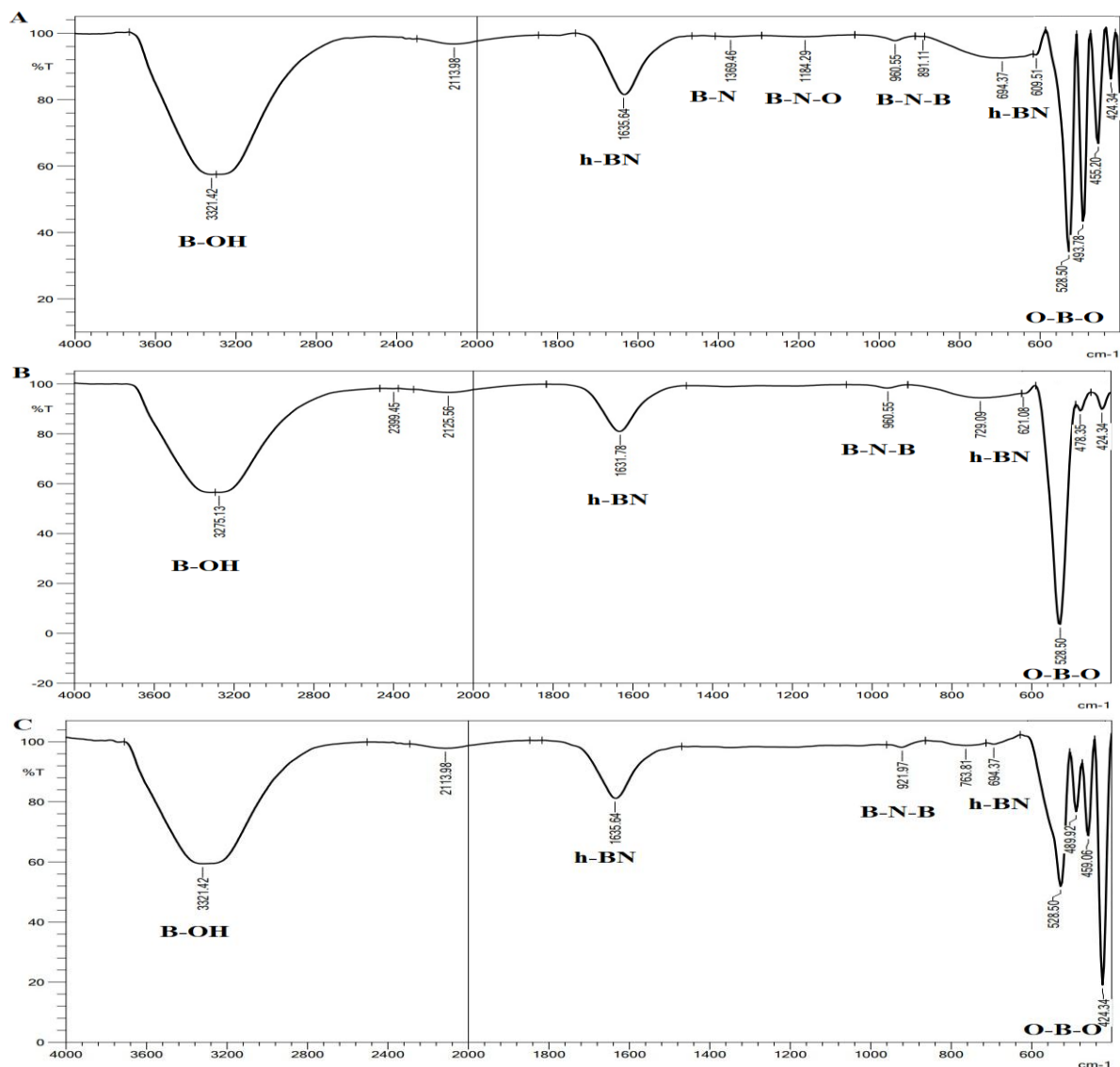


Figure 9: FTIR spectra of h-BNNs colloidal prepared by laser fragmentation by 532 nm and different laser energy A) 10 mJ, B) 30 mJ, and C) 50 mJ.

3.4. UV/Visible Analysis

Figure 10 demonstrates how UV-visible absorption measurements were used to assess the optical properties of the h-BNNs before and after fragmentation in DDW. All absorption spectra appeared typical of h-BNNs, with consistent absorbance in the range of 200 to 500 nm and a shoulder peak between 200 and 215 nm. Additionally, absorption peaks at 205, 207, 210, and 215 nm were observed, indicating the production of h-BNNs, which falls within the ultraviolet range. This absorption peak is a result of electronic transitions within the material. The extensive contact with the solvent and a slight hump at 277, 347, and 360 nm, are believed to be caused by vacancy defects in the crystal structures of the nanoflakes and BNNTs synthesized [4]. The change in the size of h-BNNs, the impact of quantum confinement, size, and the synthesis of BNNTs are all responsible for the minor shift of the observed shoulder peak. Optical absorption between 390 and 500 nm is absent in the electromagnetic spectrum for h-BNNs. Nevertheless, they exhibit an absorption peak in the ultraviolet range (203-360 nm) [25, 26]. This unique characteristic makes h-BNNs, including nanotubes and nanosheets, an excellent choice for producing transparent films that effectively block ultraviolet radiation. The optical energy gap was determined using Tauc's relationship [27-30]. $\alpha h\nu = (h\nu - E_g)^{1/2}$, $r = 1/2$ (direct allowed transition)

$$(\alpha h\nu)^2 = (h\nu - E_g) \quad (2)$$

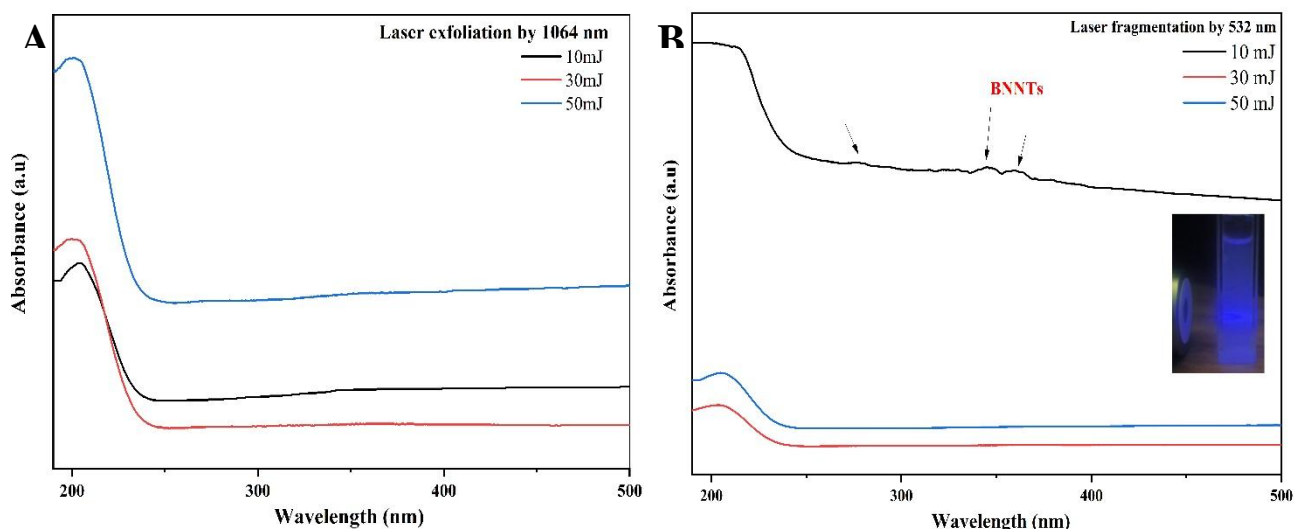


Figure 10: Optical characteristics of UV-visible absorption spectra of h-BNNs samples, prepared by A) laser exfoliation, B) laser fragmentation in liquid with different laser energy.

Figures 11 and 12 illustrate the plot of the rising edge of the energy dispersion curve against $(\alpha E)^2$ vs. E , enabling extrapolation to the energy axis. The value of E that corresponds to $(\alpha E)^2$ when it reaches 0 represents the optical band gap energy, E_g . The energy gap of a colloidal solution prepared by 1064 nm increases from 4.8 to 5.1 eV, while the energy gap of a colloidal solution prepared by 532 nm increases from 4.4 to 5 eV. However, an increase in the quantity of nanostructures in the colloidal solution corresponds to an increase in the energy gap, as confirmed by SEM investigations [27-33]. H-BNNs are typically white in color and become transparent due to their large band gap [23, 32, and 34]. When examining the absorption spectra, it is important to note that the produced h-BNNs exhibit an absorption edge in the UV range. Furthermore, an increase in laser fluence leads to a blue shift in the absorption edge of the resulting products. This indicates that as laser fluence increases, particle size reduction causes quantum confinement, leading to an increased energy band gap. The quantum confinement effect confines electrons and holes at a nanoscale level, bringing them closer together and making the coulombic interaction between them negligible. As a result, there is higher kinetic energy and an increase in the energy difference between filled and empty states, ultimately widening the semiconductor's band gap [35].

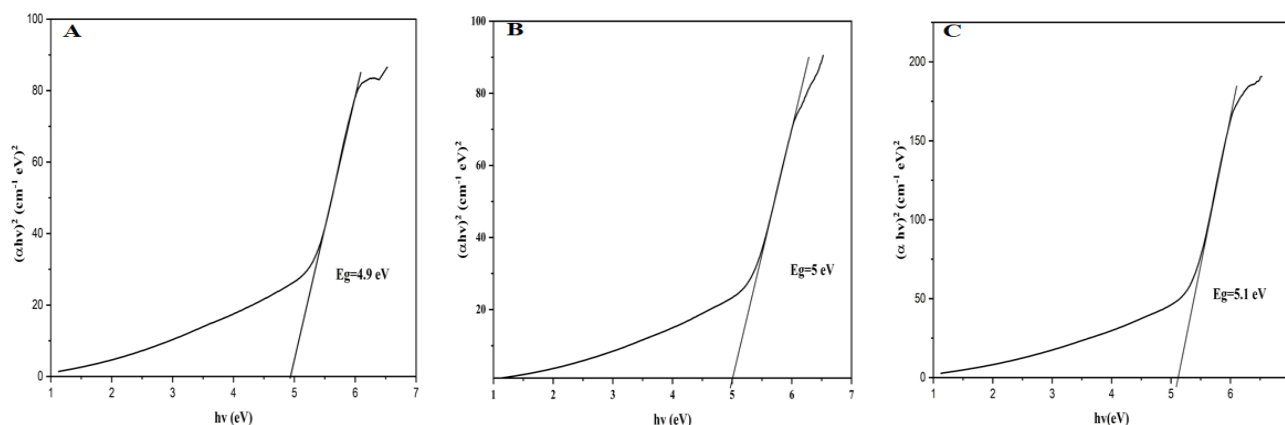


Figure 11: Optical the band gap of h-BNNs colloidal prepared by laser exfoliation by 1064 nm and different laser energy A) 10mJ, B) 30 mJ, and C) 50mJ.

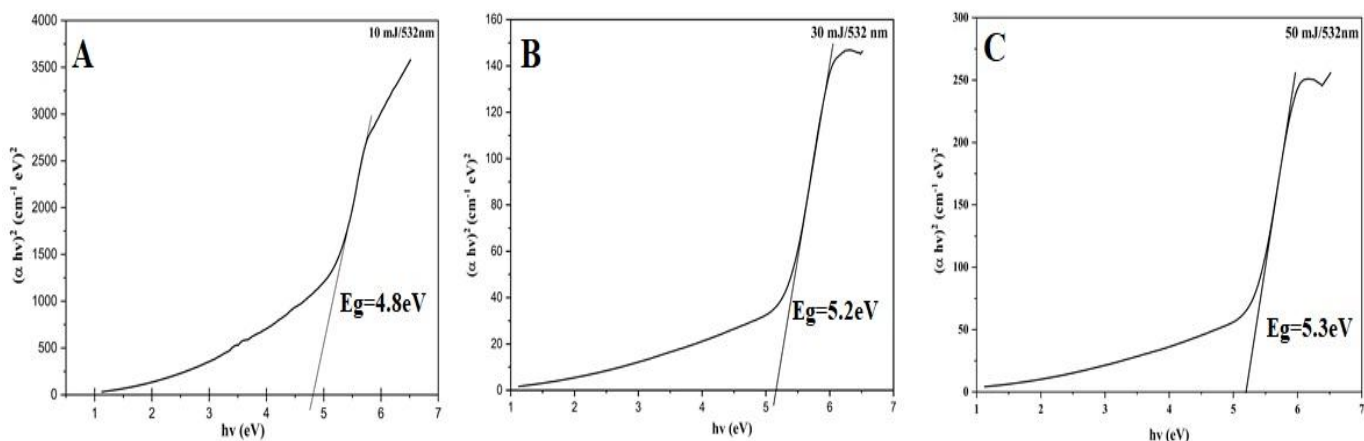


Figure 12: Optical the band gap of h- BNNs colloidal prepared by laser fragmentation by 532 nm and different laser energy A) 10mJ, B) 30 mJ, and C) 50mJ.

3.5. Fluorescence Emission

When h-BNNs colloidal samples were created by laser exfoliation and fragmentation in DDW with two wavelengths, and 10mJ, they were given an excitation wavelength of 220, 265, and 365 nm. This emission's reaction was measured in the 250–600 nm range. In Figure 13, the observed UV emission in h-BNNs at a wavelength of 375 nm can be explained by its unique band gap of 4.8 eV, which corresponds to deep ultraviolet wavelengths.

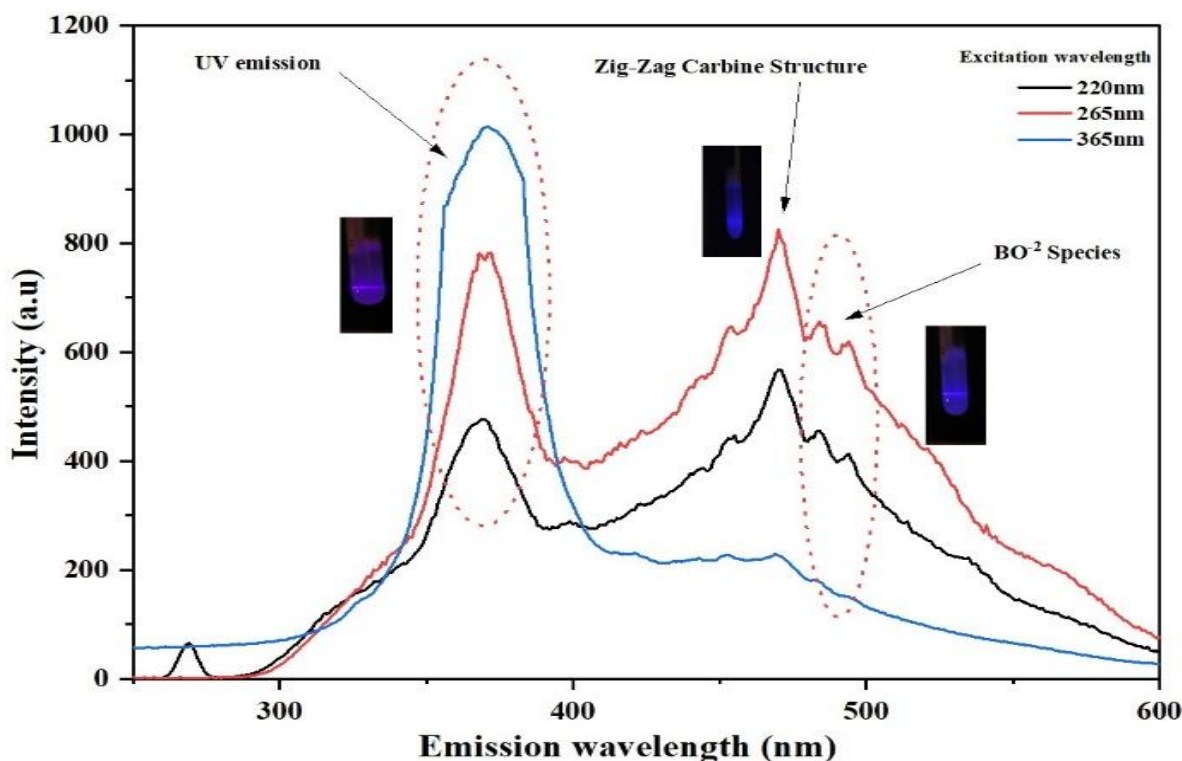


Figure 13: Fluorescence spectra of h-BNNs prepared by laser fragmentation in DDW with 532 nm and 10 mJ at an excitation of 220, 265, and 365 nm. In the inset, the luminescence of the sample is under UV light.

Table 3: Comparison between exfoliation by laser exfoliation and fragmentation and other exfoliation method.

Exfoliation	starting	Time	Scalable	Product size	Mechanism	Degree of	reference
-------------	----------	------	----------	--------------	-----------	-----------	-----------

method	material	(hour)	parameters			Exfoliation	
Laser exfoliation and fragmentation in liquid(LEFL)	Powder suspension	<0.25h	Sonication time; solvent; laser energy; laser wavelength; pulse frequency; irradiation time; liquid volume;	Laser parameters can be finely tuned to control the size and thickness of the BN nanosheets produced.	Use of a high-powered laser to ablate or vaporize a bulk BN material, leading to the formation of BN nanosheets or nanoparticles. The laser energy breaks the interatomic bonds within the BN structure, causing exfoliation into smaller layers.	Highly exfoliated BN nanosheets with fewer defects due to the localized energy input.	This work
Laser-assisted exfoliation	crystal; powder suspension	<0.5 h	solvent; laser energy; laser wavelength; pulse frequency; irradiation time; liquid volume;				[40]
Sonication	powder suspension	>3 h	solvent; sonication power; liquid volume; time	These methods may offer less precise control over the size, and thickness of the BN nanosheets.	In mechanical exfoliation, bulk BN is mechanically sheared or peeled using adhesive tapes or other mechanical means to obtain thin layers or nanosheets.	These methods may result in a wider range of exfoliation degrees, with the possibility of increased defects and impurities in the BN nanosheets.	[41]
Ball-milling	powder; powder suspension	>10 h	solvent; revolution speed; ball size; ball-filling ratio; volume; time				[42]
Hydrothermal	powder suspension	>1 h	solvent; chemical species; temperature; liquid volume; time		Chemical exfoliation relies on the use of chemical agents to break the interlayer bonding in bulk BN, resulting in the formation of BN nanosheets.		[43]
Microwave-assisted	powder suspension	<1 h	solvent; microwave energy; microwave frequency; chemical species; liquid volume; time				[44]
Direct electrochemical	conductive Crystal	<1 h	solvent; chemical species; potential; temperature; liquid volume; time				[45]

This emission is associated with excitonic transitions, where electron-hole pairs are bound together by the Coulomb interaction. When an electron is excited from the valence band to the conduction band, an exciton forms as a result of the generated hole. The recombination of these excitons produces photons, resulting in the observed UV emission. Additionally, UV emission can be influenced by quantum confinement effects. As the size of h-BNNs decreases, the confinement of charge carriers causes the electronic states to become quantized. This quantum confinement alters the electronic band structure, leading to changes in energy levels and allowing for tunable UV emission. About 470–474 nm, a robust emission peak is observed from various excitation wavelengths, indicating the presence of Doping of the oxygen atom in h-BNNs. This emission peak was previously attributed to zigzag carbene structures that caused fluorescence behavior in a white graphene-like system, resulting in quantum confinement. However, the presence of contaminants in the sample produces a hump at 485 nm, likely due to the small amount of BO₂ impurity confirmed by FTIR spectra. BO₂- species can

release blue emission as an impurity in the h-BNNs structure. The nanoflake exhibits a dominant emission peak at 415 nm in the fluorescence spectra, resulting from the confinement of quantum states within the zigzag carbene structure. This emission is highly influential, as it signifies the transition from the highest occupied molecular orbital (HOMO) to the orbitals of the lowest occupied molecular orbital (LUMO). The presence of zigzag edges with a triplet ground state, similar to a carbene, characterizes this transition [36-39]. The electronic properties and photocatalytic characteristics of h-BN nanoparticles can be significantly altered by the existence of surface oxygen vacancies, resulting in modifications to their band gap. Based on our findings, it is evident that the exfoliation of Boron Nitride (BN) using laser and other methods involves unique processes and mechanisms, leading to variations in the properties and characteristics of the resulting BN nanomaterials. The disparities between laser exfoliation and other commonly used methods are summarized in Table 3.

4. Conclusions

In summary, we have developed a straightforward method for producing h-BNNs using nanosecond laser pulses and probe sonication-assisted exfoliation. Without the use of surfactants, we successfully achieved exfoliation and fragmentation of bulk BN powder in DDW. This resulted in the generation of three distinct samples of h-BNNs. Our study primarily focused on investigating the effects of laser energy and wavelength on the nanostructure, shape, and optical properties of these nanomaterials. The hexagonal structure of the nanoparticles was confirmed through X-ray diffraction (XRD) and selected area electron diffraction (SAED) tests, where the diffraction peak corresponding to pure h-BN was observed at 26.7° (002). The crystallite size was determined to be in the range of 11-18 nm. Interestingly, we observed various types of nanostructures, including disk-like, spherical, rod-like, and sheet-like shapes, which could be attributed to variations in laser energy and wavelength during synthesis. Moreover, the optical band gap energy (E_g) was measured to be between 4.9-5.1 eV for samples synthesized using a 1064 nm laser, and between 4.8-5.3 eV for samples synthesized using a 532 nm laser. Furthermore, the fluorescence spectra exhibited three distinct peaks at wavelengths of 375 nm, 470 nm, and 485 nm, indicating the presence of fluorescent emissions in the h-BNNs samples. Laser exfoliation of BN offers advantages in terms of precision and reduced defects but may have limitations in scalability and energy efficiency.

Acknowledgement

The authors would like to thank the University of Technology, Baghdad, Iraq, and the University of Bisha, Saudi Arabia, for technical, instrumental, and infrastructural support during this study.

Conflict of Interest

The authors declare that they have no conflict of interest.

References

- [1] H. Li, R. Y. Tay, S. H. Tsang, X. Zhen, and E. H. T. Teo, "Controllable synthesis of highly luminescent boron nitride quantum dots", *Small*, vol. 11, no. 48, pp. 6491-6499, 2015.
- [2] S. N. Rashid, K. A. Aadim, A. S. Jasim, and A. M. Hamad, "Synthesized zinc nanoparticles via pulsed laser ablation: characterization and antibacterial activity", *Modern Science.*, vol.8, no. 3, pp. 17, 2022.
- [3] S. Angizi, M. Khalaj, S. A. A. Alem, A. Pakdel, M. Willander, A. Hatamie, and A. Simchi, "Towards the two-dimensional hexagonal boron nitride (2D h-BN) electrochemical sensing platforms", *Journal of The Electrochemical Society*, vol. 167, no. 12, pp. 126513, 2020.
- [4] V. Nguyen, L. Yan, N. Zhao, N. Van Canh, N. T. N. Hang, and P. H. Le, "Tuning photoluminescence of boron nitride quantum dots via surface functionalization by femtosecond laser ablation", *Journal. Of Molecular Structure*, vol. 1244, pp. 130922, 2021.
- [5] B. Podgornik, T. Kosec, A. Kocijan, and Č. Donik, "Tribological behavior and lubrication performance of hexagonal boron nitride (h-BN) as a replacement for graphite in aluminum forming", *Tribology International*, vol. 81, pp. 267-275, 2015.
- [6] C. Gautam, A. Gautam, V. K. Mishra, N. Ahmad, R. Trivedi, and S. Biradar, "3D interconnected architecture of h-BN reinforced ZrO₂ composites: structural evolution and enhanced mechanical properties for bone implant applications", *Ceramics International*, vol. 45, no. 1, pp.1037-1048, 2019.

- [7] A. Gautam, C. Gautam, U. Kumar, and B. C. Yadav, "Synthesis and structural investigations of microporous graphene reinforced h-BN solids for LPG sensing applications", *Materials Research Express*, vol. 6, no. 12, pp. 125090, 2019.
- [8] L. Cao, S. Emami, and K. Lafdi, "Large-scale exfoliation of hexagonal boron nitride nanosheets in the liquid phase", *Materials Express*, vol. 4, no. 2, pp. 165-171, 2014.
- [9] D. Zhang, Z. Li, and K. Sugioka, "Laser ablation in liquids for nanomaterial synthesis: diversities of targets and liquids", *Journal. Physics: Photonics*, vol. 3, no. 4, pp. 042002, 2021.
- [10] S. J. An, Y. H. Kim, C. Lee, D. Y. Park, M. S. Jeong, "Exfoliation of transition metal dichalcogenides by a high-power femtosecond laser", *Scientific reports*, vol. 8, no. 1, pp. 12957, 2018.
- [11] V. Nguyen, J. Si, L. Yan, and X. Hou, "Electron-hole recombination dynamics in carbon nanodots", *Carbon*, vol. 95, pp. 659-663, 2015.
- [12] M. H. Mohsin, K. S. Khashan, and G. M. Sulaiman, "Optical and Structural Properties of H-BN@ Gd₂O₃ Nanoflake Prepared by Laser-Induced Ablation in Liquid", *Physica Scripta*, vol. 98, no. 5, pp. 055903, 2023.
- [13] Z. Rafiei Sarmazdeh, S. H. Jafari, Ahmadi, S. J. Jafari, and S. M. Zahedi-Dizaji, "Large-scale exfoliation of hexagonal boron nitride with combined fast quenching and liquid ex-foliation strategies", *Journal. Materials Science*, vol. 51, no. 6, pp. 3162-3169, 2016.
- [14] A. Kumar, G. Malik, S. Sharma, R. Chandra, and R. S. Mulik, "Precursors controlled morphologies of nanocrystalline h-BN and its growth mechanism", *Ceramics International*, vol. 47, no. 21, pp. 30985-30992, 2021.
- [15] Z. Lei, S. Xu, J. Wan, and P. Wu, "Facile preparation and multifunctional applications of boron nitride quantum dots", *Nanoscale*, vol. 7, no. 45, pp. 18902-18907, 2015.
- [16] A. Olszyna, J. Konwerska Hrabowska, and M. Lisicki, "Molecular structure of E-BN", *Diamond and Related Materials*, Vol. 6, no. 5-7, pp. 617-620, 1997.
- [17] M. Kim, S. Osone, T. Kim, H. Higashi, and T. Seto, "Synthesis of nanoparticles by laser ablation: A review", *J. KONA Powder and Particle*, vol. 34, pp. 80-90, 2017.
- [18] M. A. Domínguez-Crespo, E. Rodríguez, A. M. Torres-Huerta, I. J. Soni Castro, S. B. Narro-García, R. Brachetti-Sibaja, and A. B. López-Oyama, "Production of BN nanostructures by pulsed laser ablation in liquids: influence of the applied Nd: YAG harmonics on the structural, optical and photoluminescence properties", *Ceramics International*, vol. 46, no. 13, pp. 21667-21680, 2020.
- [19] K. S. Khashan, G. M. Sulaiman, and S. A. Hussain, "Synthesis and characterization of aluminum doped zinc oxide nanostructures by Nd: YAG laser in liquid", *Iraqi Journal of Science*, pp. 2590-2598, 2020.
- [20] K. S. Khashan, and M. H. Mohsin, "Characterization of carbon nitride nanoparticles prepared by laser ablation in liquid for optoelectronic application", *Surface Review and Letters*, vol. 22, no. 4, pp. 1550055, 2015.
- [21] G. Ciofani, S. Danti, G. G. Genchi, B. Mazzolai, and V. Mattoli, "Boron nitride nanotubes: Biocompatibility and potential spill-over in nanomedicine", *Small*, vol. 9, no. 9-10, pp. 1672-1685, 2013.
- [22] X. Chen, P. Wu, M. Rousseas, D. Okawa, Z. Gartner, A. Zettl, and C. R. Bertozzi, "Boron nitride nanotubes are noncytotoxic and can be functionalized for interaction with proteins and cells", *Journal. Of the American Chemical Society*, vol. 131, no. 3, pp. 890-891, 2009.
- [23] A.S. Lansy, T. A. Saeed, R. Al-Attar, Y. Guo, Y. Yang, B. Liu, and Z. Fan, "Boron nitride nanosheets modified with zinc oxide nanoparticles as novel fillers of dental resin composite", *Dental Materials*, vol. 38, no. 10, pp. e266-e274, 2022.
- [24] V. Kumar, K. Nikhil, P. Roy, D. Lahiri, and I. Lahiri, "Emergence of fluorescence in boron nitride nanoflake and its application in bioimaging", *RSC advances*, vol. 6, no. 53, pp. 48025-48032, 2016.
- [25] L. H. Li, Y. Chen, "Atomically thin boron nitride: unique properties and applications", *Advanced Functional Materials*, vol. 26, no. 16, pp. 2594-2608, 2016.
- [26] Y. Song, C. Zhang, B. Li, D. Jiang, G. Ding, H. Wang, and X. Xie, "Triggering the atomic layers control of hexagonal boron nitride films", *applied surface science*, vol. 313, pp. 647-653, 2014.
- [27] H. Nasiri, D. Dorranean, A. H. Sari, "Green laser assisted gold-iron oxide nanocomposite production", *Radiation Effects and Defects in Solids*, vol. 177, no. 3-4, pp. 277-293, 2022.

- [28] I. F. Hasan, K. S. Khashan, A. A. Hadi, "Study of the effect of laser energy on the structural and optical properties of TiO₂ NPs prepared by PLAL technique", *Journal of Applied Sciences and Nanotechnology*, vol. 2, no. 1, pp. 11-19, 2022.
- [29] R. Al-Obaidy, A. J. Hadier, S. Al-Musawi, N. Arsad, "Study of the Effects of Solution Types on Concentration of Iron Oxide by Pulsed Laser Ablation in Liquid", *Journal of Applied Sciences and Nanotechnology*, vol. 3, no. 1, pp. 137-150, 2023.
- [30] P. R. Jubu, F. K. Yam, V. M. Igba, K. P. Beh, "Tauc-plot scale and extrapolation effect on bandgap estimation from UV-vis-NIR data—a case study of β -Ga₂O₃", *Journal of Solid State Chemistry*, vol. 290, pp. 121576, 2020.
- [31] M. S. Alwazny, R. A. Ismail, E. T. Salim, "Optical Properties of Lithium Niobate Nanoparticles Prepared by Laser Ablation in Different Surfactant Solutions", *Journal of Applied Sciences and Nanotechnology*, vol. 3, no. 1, 2023.
- [32] S. Bhatia, A. Khanna, "Structural and optical properties of molybdenum trioxide thin films", In AIP Conference Proceedings, AIP Publishing LLC, Vol. 1665, No. 1, p. 080057, 2015.
- [33] S. Angizi, F. Shayeganfar, M. H. Azar, A. Simchi, "Sur-face/edge functionalized boron nitride quantum dots: Spectroscopic fingerprint of bandgap modification by chemical functionalization", *Ceramics International*, vol. 46, no. 1, pp. 978-985, 2020.
- [34] W. Meng, Y. Huang, Y. Fu, Z. Wang, C. Zhi, "Polymer composites of boron nitride nanotubes and nanosheets", *Journal. Materials Chemistry C*, vol. 2, no. 47, pp. 10049-10061, 2014.
- [35] K. S. Khashan, G. M. Sulaiman, and R. Mahdi, "The effect of laser energy on the properties of carbon nanotube iron oxide nanoparticles composite prepared via pulsed laser ablation in liquid", *Materials Research Express*, vol. 5, no. 10, pp. 105004, 2018.
- [36] M. Singh, M. Goyal, K. Devlal, "Size and shape effects on the band gap of semiconductor compound nanomaterials", *Journal of Taibah University for Science*, vol. 12, no. 4, pp. 470-475, 2018.
- [37] L. Xu, Y. Peng, Z. Meng, W. Yu, S. Zhang, X. Liu, Y. Qian, "A co-pyrolysis method to boron nitride nanotubes at relatively low temperature", *Chemistry of Materials*, vol. 15, no. 13, pp. 2675-2680, 2003.
- [38] N. S. Dawood, M. Q. Zayer, and M. F. Jawad, "Preparation and Characteristics Study of Porous Silicon for Vacuum Sensor Application", *Karbala International Journal of Modern Science*, vol. 8, no. 1, pp. 105-113, 2022.
- [39] A. K. Ali, S. Erten-Ela, R. A. Ismail, C. Yavuz, "Preparation of blue luminescence gold quantum dots using laser ablation in aromatic solvents", *Applied Nanoscience*, vol. 11, pp. 2779-2791, 2021.
- [40] W. Zheng, J. Lee, Z.W. Gao, Y. Li, S. Lin, S.P. Lau, L.Y.S. Lee, "Laser-assisted ultrafast exfoliation of black phosphorus in liquid with tunable thickness for Li-ion batteries", *Adv. Energy Mater*, vol. 10, pp. 1903490, 2020.
- [41] S. Shaybanizadeh, A. N. Chermahini, "Fabricating boron nitride nanosheets from hexagonal BN in water solution by a combined sonication and thermal-assisted hydrolysis method", *Ceramics International*, vol. 47, no. 8, pp. 11122-11128, 2021.
- [42] Z. P. Xia, Z. Q. Li, "Structural evolution of hexagonal BN and cubic BN during ball milling", *Journal of alloys and Compounds*, vol. 436, no. 1-2, pp. 170-173, 2007.
- [43] S. Kumari, A. Chouhan, O. P. Sharma, S. A. Tawfik, M. J. Spencer, S. K. Bhargava, O. P. Khatri, "Alkali-assisted hydrothermal exfoliation and surfactant-driven functionalization of h-BN nanosheets for lubrication enhancement", *ACS Applied Nano Materials*, vol. 4, no. 9, pp. 9143-9154, 2021.
- [44] L. Fu, G. Lai, G. Chen, C. T. Lin, A. Yu, "Microwave Irradiation-Assisted Exfoliation of Boron Nitride Nanosheets: A Platform for Loading High Density of Nanoparticles", *Chemistry Select*, vol. 1, no. 8, pp. 1799-1803, 2016.
- [45] I. Fatima, O. Fayyaz, M. M. Yusuf, Al-Ashrafhraf, R. A. Shakoor, "Enhanced electrochemical and mechanical performance of BN reinforced Ni-P based Nanocomposite coatings", *Diamond and Related Materials*, vol. 130, pp. 109454, 2022.